Fracture 1977, Volume 2, ICF4, Waterloo, Canada, June 19 - 24, 1977

EFFECT OF GRAIN SIZE AND γ' SIZE ON FATIGUE CRACK PROPAGATION IN RENE 95

J. Bartos* and S. D. Antolovich**

INTRODUCTION

Nickel base alloys are a highly complex family of materials utilized principally for applications requiring high strength as well as resistance to creep and fatigue at high temperatures. In the temperature range of 773 - 923 K perhaps the most important property is fatigue resistance. Cyclic loading can cause crack formation at net section stresses below yield. This problem is of course exacerbated at notches. These flaws will then eventually propagate to failure. An understanding of the basic metallurgical processes is important if optimum alloys and heat treatments are to be employed where resistance to FCP is critical.

René 95 was chosen as being typical of the complex high strength superalloys currently being used in gas turbines.

EXPERIMENTAL PROCEDURE

The basic material from which test specimens were made was in the form of -60 mesh powder, which was consolidated at 1393 K at an Ar pressure of 103 MPa. The compact was then held for three hours to insure densification. After HIPing, blanks were cut and heat treated according to the schedule shown in Table 1. The blanks were then machined into CT specimens 63.5 mm thick. FCP testing was carried out at 811 K and at a frequency of 0.33 Hz using a closed loop servo hydraulic test machine. The crack length was measured optically using a travelling vernier microscope and to facilitate this cycling was periodically interrupted. In addition to the FCP test, standard tensile tests were also carried out.

RESULTS AND DISCUSSION

A. Heat Treatment

A typical as HIPed microstructure is shown in Figure 1. The HIP temperature never exceeded the solvus (1436 K) and a fraction of the 48 V% γ' remained undissolved and homogeneously distributed, serving as a pinning agent to prevent excessive grain growth. The grain size of the HIP product remained at 5 - 10 μm diameter during HIP.

* General Electric Aircraft Engine Group, Evendale, Ohio 45215, U. S. A.
**Department of Materials Science, University of Cincinnati, Cincinnati, Ohio 45221, U. S. A.

The principal objectives of the heat treatment were to produce two grain sizes, each containing 5 different γ' size/spacing combinations. A representative coarse grained microstructure is shown in Figure 2.

The heat treatments [1] were such that identical volume fractions of γ' were present in all specimens.

B. Tensile

The yield stress as a function of γ' size is shown in Figure 3 for both grain sizes. The curves suggest that Orowan looping is the primary hardening mechanism [2] for small γ' sizes (i.e., $d\gamma' < 0.3$ μm) and that grain size effects on strength are significant only when this mechanism becomes inoperative.

C. FCP

The data were represented in the form of a Paris equation [3]

$$\frac{da}{dN} = R(\Delta K)^m \quad . \tag{1}$$

All specimens for which the standard error of regression was greater than 0.1 were excluded. In general, there was excellent agreement among duplicate specimens. Results are given in Table 2. The effects of microstructural parameters on m are shown in Figure 4. These results indicate a significant effect of γ' size on m, particularly for small sizes in the coarse grained specimens. The clear grain size effect on m is in apparent disagreement with a number of theories and observations [4, 5, 6]. The data of Table 3 indicate that the major effect of microstructures on rate occurred in the low ΔK regime. These results would be intuitively expected since the plastic zone is small and of the same size order as the microstructure. The real practical effect of microstructure is shown in Figure 5 where the residual life between 30 and 66 MPa $m^{1/2}$ is given. Note that this curve is nearly identical in form to that of Figure 4, implying that the residual life, for reasonable ranges of ΔK, increases with m.

D. Fractography and Transmission Microscopy

Considerable fractographic examinations were carried out and the various mechanisms observed are indicated in Table 3. Typical fractographs are shown in Figure 6 for coarse grained specimens at low ΔK levels (where the microstructural effects were the greatest). With large γ' (Figure 6a) cracking is transgranular with striation formation along with intergranular and crystallographic branch cracks. There is a dramatic change in the fracture appearance for the fine γ' (Figure 6b). In this case, fracture appears to have proceeded transgranularly by a stage I mechanism. This effect is shown more clearly in Figure 7 which was taken from the fracture surface of an LCF strain control specimen at $\Delta\varepsilon_p = 0.25\%$. This mode of fracture is commonly observed in Ni base alloys at $T < Tm/2$ and is generally associated with lower crack growth rates [9, 10].

Some TEM studies were carried out, but due to the relatively small reversed plastic zone sizes, it was questionable whether or not foils were taken from within the plastic enclave. However foils taken from LCF specimens containing fine γ' exhibited both planar slip band formation (presumably along with some shearing) as well as particle looping. On the other hand, coarse γ' appeared to lead to a more cell-like dislocation substructure with dislocations being "stored" on the large γ' particles. Representative micrographs are shown in Figures 8 and 9. It is clear that the deformation mode is a function of microstructure and this is in turn reflected in the FCP properties.

E. Analysis of FCP Mechanisms

The experimental observations can be interpreted in terms of a model proposed by Antolovich and Saxena [11, 12]. They showed that:

$$\frac{da}{dN} \simeq 4\left(\frac{0 \cdot 7C}{\sigma_{ys}\varepsilon_f E}\right)^{\frac{1}{\beta}} \cdot \frac{1}{\ell^{1-\beta/\beta}} \cdot (\Delta K)^{\frac{2}{\beta}} \quad , \tag{2}$$

where β is the exponent in the Coffin-Manson LCF equation, ℓ is a process zone ahead of the crack tip and C is related to the plastic zone size in fatigue by the equation:

$$R_p^f \simeq C\left(\frac{\Delta K}{\sigma_{ys}}\right)^2 \quad . \tag{3}$$

This has the form of the Paris equation and has the advantage of being more fundamental for purposes of analysis.

Antolovich and Saxena found that $C \simeq 1/24\pi$. They further found that the cyclic strain hardening exponent n' is related to the Paris exponent:

$$m = 2\alpha\,(n'+1) \quad , \tag{4}$$

where α is a parameter that depends on slip mode. For wavy slip $\alpha > 1$, while for planar slip $\alpha \to 1$. Using appropriate mechanical property data, ℓ values can be calculated that are very close to the interprecipitate spacings in all cases. For example, in the fine grain/small γ' specimens, the calculated $\ell \sim 0.20$ μm, is very close to the interprecipitate spacing. The large values of the Paris exponent for fine γ' can be explained in terms of increased strain hardening and subsequent slip dispersal. This is desirable at low ΔK levels since the rate will drop off drastically leading to longer lives (Figure 5). The experimental results were analyzed in terms of several other models [13 - 21], but in no instance was it possible to obtain the same degree of agreement that was obtained using the above indicated model.

SUMMARY AND CONCLUSIONS

1. Grain size and γ' size significantly affect FCP in René 95 at 811 K. Grain size influences the preferred crack propagation mechanism while γ' size controls deformation characteristics.

2. FCP decreases with decreasing γ' particle size (greater strain hardening) in materials exhibiting predominantly transgranular (stage I) fracture due to slip dispersal at the crack tip. da/dN is independent of γ' particle size for $\gamma' > 0.2$ μm diameter (reduced strain hardening).

3. Additional crack propagation mechanisms, such as slip band cracking, intergranular fracture, cleavage or secondary branch cracking, become operative when the plastic zone diameter at the crack tip equals or exceeds the average grain diameter of the material.

These additional propagation modes accelerate da/dN to levels beyond those predicted by FCP models based on a single mechanism.

4. Crack propagation behaviour can be described by the FCP law:

$$\frac{da}{dN} = R(\Delta K)^m .$$

Microstructural parameters can be related to da/dN in strain hardening materials exhibiting transgranular fracture by using equations (2) - (4). The structural process zone, ℓ, is in the order of the γ' interparticle spacing.

5. The exponent in the FCP equation, m, increases as γ' particle size decreases for γ' particles < 0.2 μm diameter (increased strain hardening). The residual cyclic life in the range ΔK = 30 to ΔK = 66 MPa $m^{1/2}$, also increases with increasing m.

6. The effect of microstructure on FCP rate is strongest at low stress intensities. The large plastic zones at crack tips created by high stress intensities tend to minimize microstructural effects at higher levels.

REFERENCES

1. BARTOS, J., Ph. D. Dissertation, University of Cincinnati, 1976.
2. STOLOFF, N. S., "The Superalloys", 1972, 79.
3. PARIS, P. C., "Proceedings of the 10th Sagamore Army Mat. Res. Conf.", Syracuse Univ. Press, Syracuse, New York, 1964.
4. PELLOUX, R. M., "16th Sagamore Conference on Ultrafine Grain Materials", 1969, 231.
5. MERRICK, H. F., MAXWELL, D. H. and GIBSON, R. C., ASTM STP 520, 1973, 285.
6. MERRICK, H. F., Met. Trans., 5, 1974, 891.
7. WELLS, C. H., SULLIVAN, C. P. and GELL, M., ASTM STP 495, 1971, 61.
8. GROSSKRUETZ, J. C., ASTM STP 495, 1971, 5.
9. LAIRD, C., ASTM STP 415, 1967, 131.
10. GELL, M., LEVERANT, G. R. and WELLS, C. H., ASTM STP 467, 1970, 113.
11. ANTOLOVICH, S. D., SAXENA, A. and CHANANI, G. R., Eng. Fract. Mech., 7, 1975, 649.
12. SAXENA, A. and ANTOLOVICH, S. D., Met. Trans., 6A, 1975, 1809.
13. HEAD, A. K., Phil. Mag., 44, 1953, 925.
14. McCLINTOCK, F. A., "Fracture of Solids", John Wiley, New York, 1963, 65.
15. TOMPKINS, B., Phil. Mag., 18, 1968, 1041.
16. ERDOGAN, F., "Fracture: An Advanced Treatise", 1968, 497.
17. McEVILY, A. J. and JOHNSTON, T. L., "Proceedings of the First Conf. on Fracture", Vol. II, Japanese Society for Strength and Fracture of Materials, 1965.

18. KRAFT, J. M., Paper presented to ASTM Committee E24, 1964.
19. FROST, N. E. and DIXON, J. R., Int. J. Fract. Mech., 3, 1967, 301.
20. PEARSON, S., Nature, 211, 1966, 1077.
21. MILLER, G. A. and THROOP, J. F., Paper presented to ASTM National Meeting, Atlantic City, New Jersey, 1969.

Table 1 Composition and Heat Treatment

SOLUTION TREATMENT	AGEING* TREATMENTS	γ' SIZE	DESIGNATION
(a) 1464 K/4 hr + 1422 K/1 hr + 0.Q (gives 30 - 50 μm grain size-denoted C)	1144 K/1 hr	0.08 μm	A
	1144 K/8 hrs	0.1 μm	B
	1144 K/72 hrs	0.2 μm	C
(b) 1422 K/1 hr + 0.Q (gives 5 - 10 μm grain size-denoted F)	1255 K/24 hrs	0.3 μm	D
	1255 K/ 72 hrs	0.5 μm	E

Composition (wt %)
Major Alloying Elements: 0.066 C, 13.2 Cr, 8.18 Co, 3.46 Al, 2.59 Ti, 3.52 Mo, 3.67 W, 3.53 Cb, 0.067 Zr, 0.011 B, Balance Ni

Impurity Elements (ppm): 65 O, 10 N, 5 H, 800 Fe, 100 Mn, 100 Si, 50 P, 20 S.

* All Specimens Brine Quenched After Ageing

Table 2 Fatigue Crack Propagation Constants $\frac{da}{dN} = R(\Delta K)^m$

Specimen Code	R*	m	Standard Error of Regression
F-A-1	7.9×10^{-11}	2.4	0.095
F-A-1	2.1×10^{-11}	2.8	0.073
F-B-1	1.8×10^{-11}	2.9	0.097
F-C-1	2.6×10^{-9}	1.6	0.074
F-C-2	8.9×10^{-10}	1.9	0.146
F-D-1	1.9×10^{-9}	1.6	0.247
F-E-1	6.2×10^{-11}	2.5	0.087
F-E-2	2.2×10^{-9}	1.6	0.057
C-A-1	6.9×10^{-14}	4.1	0.116
C-A-2	7.0×10^{-15}	4.7	0.079
C-B-1	4.4×10^{-13}	3.8	0.099
C-B-2	1.0×10^{-13}	4.2	0.100
C-B-3	6.4×10^{-14}	4.3	0.133
C-C-1	8.0×10^{-11}	2.5	0.076
C-D-1	6.7×10^{-10}	2.0	0.105
C-D-2	1.7×10^{-10}	2.3	0.109
C-E-1	3.7×10^{-10}	2.1	0.077

* when a in meters and ΔK in MPa $m^{1/2}$

Table 3 Effect of Microstructure on $\frac{da}{dN}$ and FCP Mechanism

Specimen Type	Average Grain Size, μm	Average γ' Particle Size, μm	$\frac{da}{dN} \times 10^8$ (FCP Mechanism*) at ΔK=33	ΔK=50	ΔK=66
F-A	5 - 10	0.08	36 (B)	102 (G)	216 (G)
F-B	5 - 10	0.1	41 (B)	137 (G)	305 (G)
F-C	5 - 10	0.2	71 (C)	147 (G)	241 (G)
F-D	5 - 10	0.3	58 (D)	112 (F)	178 (G)
F-E	5 - 10	0.5	58 (D)	127 (F)	229 (G)
C-A	30- 50	0.08	15 (A)	74 (B)	229 (C)
C-B	30- 50	0.1	23 (A)	122 (C)	406 (C)
C-C	30- 50	0.2	66 (B)	168 (C)	356 (C)
C-D	30- 50	0.3	71 (G)	147 (G)	267 (G)
C-E	30- 50	0.5	71 (G)	147 (G)	267 (G)

*FCP Mechanisms

(A) Primarily Transgranular
(B) Transgranular with slip band cracking
(C) Transgranular with extensive slip band cracking, cleavage, and some striations
(D) Primarily intergranular
(E) Intergranular with slip band cracking
(F) Intergranular with extensive slip band cracking, cleavage and striations
(G) Transgranular and intergranular with slip band cracking and some striations

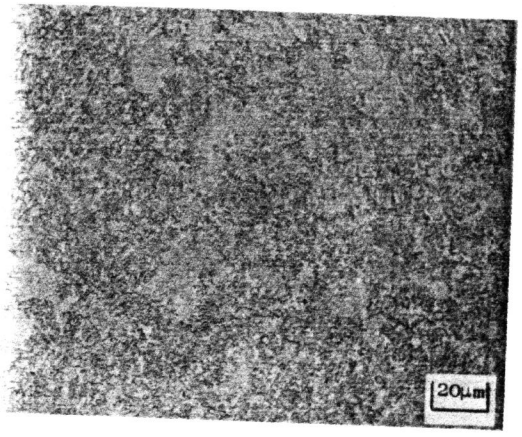

Figure 1 Microstructure of René 95 Powder Billet After HIP

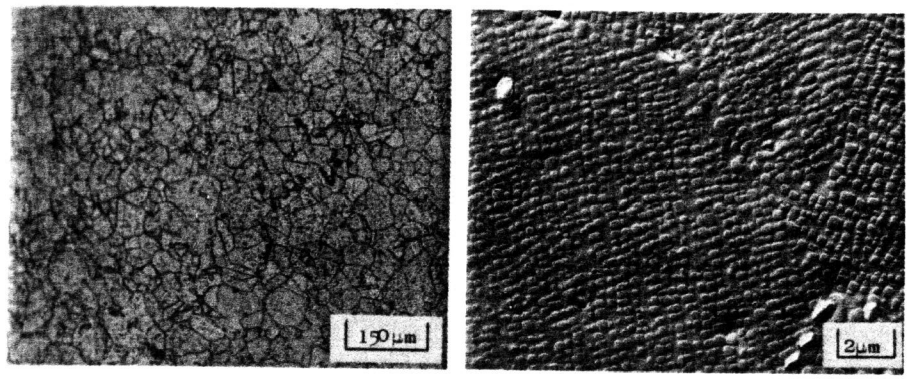

(a) (b)

Figure 2 Optical and Electron Micrographs of Specimen Aged at 1255 K for 24 hr. after Solutioning at 1464 K for 4 hr. and 1422 K for 1 hr.

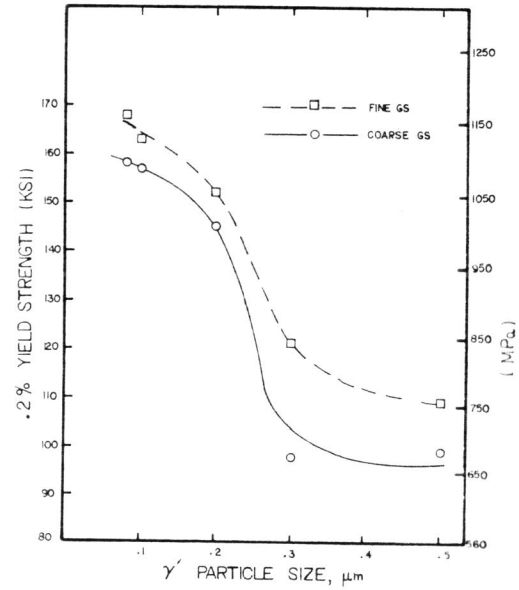

Figure 3 Effect of γ' Particle Size and Grain Size on 811 K Tensile Yield Strength.

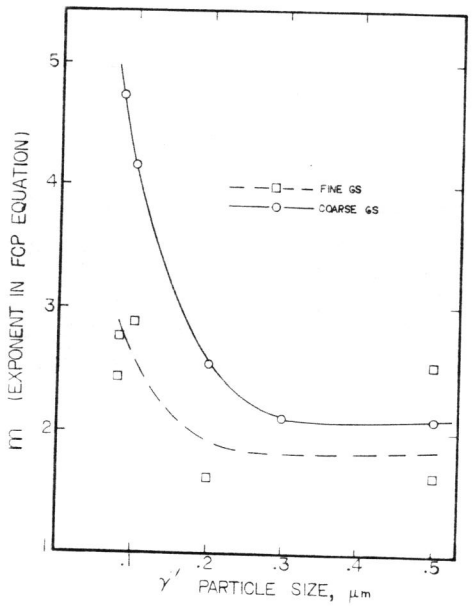

Figure 4 Effect of γ' Particle Size and Grain Size on FCP Exponent

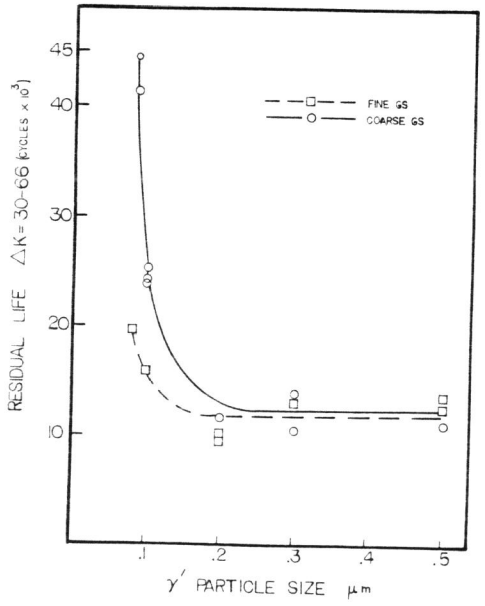

Figure 5 Effect of γ' Particle Size and Grain Size on Residual Cycle Life for ΔK = 30 to 66 MPa $m^{1/2}$

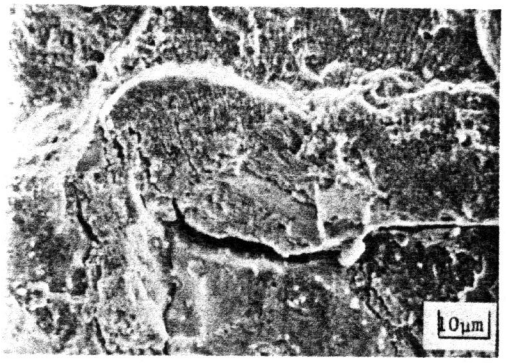

(a)

(b)

Figure 6 Fractographs of Coarse-Grained FCP Specimens at ΔK = 33 MPa $m^{1/2}$ (Crack Propagation Direction Left to Right)

(a) Specimen C-E-1 (0.5 μm γ')
(b) Specimen C-B-2 (0.1 μm γ')

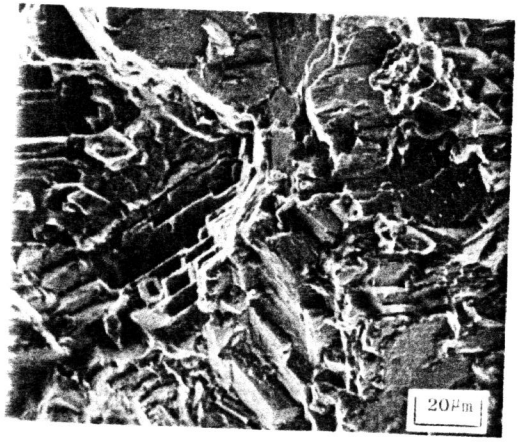

Figure 7 SEM Fractograph of Specimen LC-A-4 Tested at $\Delta\varepsilon_p$ = 0.25%

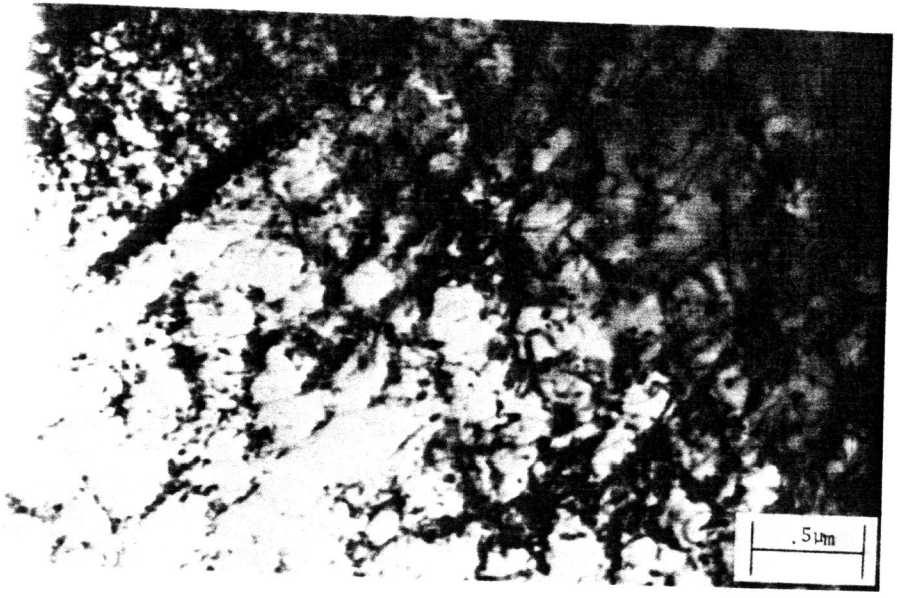

Figure 8 TEM of LCF Specimen LC-A-1 ($\Delta\varepsilon_p$ = 0.67%)

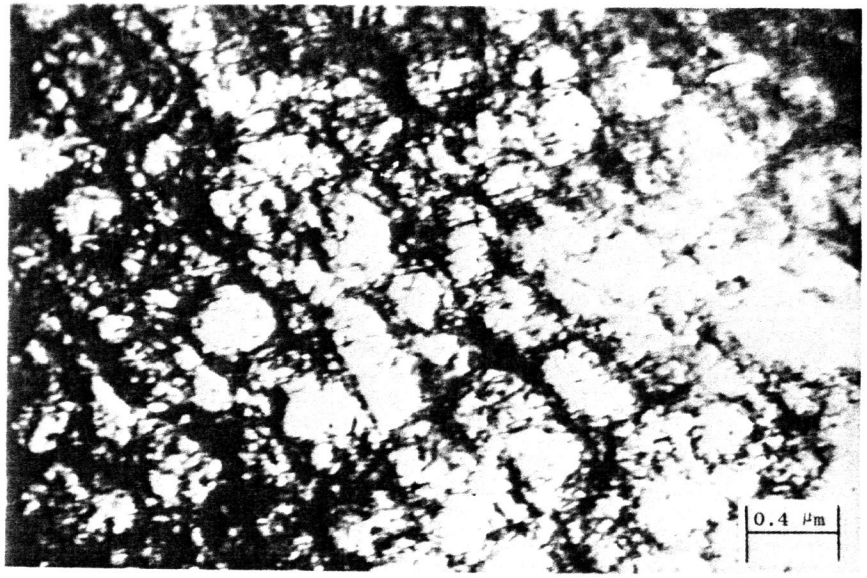

Figure 9 TEM of LCF Specimen LC-D-1 ($\Delta\varepsilon_p$ = 0.90%)